BJES Basrah Journal for Engineering Sciences

Basrah Journal for Engineering Sciences, Vol. 23, No. 1, (2023), 117-127

Original Article

Journal homepage: www.bjes.edu.iq
ISSN (Online): 23118385, ISSN (Print): 18146120

OPEN ACCESS

Comparison Between Numerical and an Experimental Results of Pressure Drop in a Perforated Horizontal Wellbore with a 90° Perforations Phasing

Mohammed A. Mustafa [1, *], Qais A. Rishack [2], Mohammed A. Abdulwahid [3]

[1] *Department of Mechanical Engineering, College of Engineering, University of Basrah, Basrah, Iraq*
[2] *Department of Material Engineering, College of Engineering, University of Basrah, Basrah, Iraq*
[3] *Department of Thermal Mechanical Engineering, Technical College, University of Southern Technical, Basrah, Iraq*
E-mail addresses: pgs2338@uobasrah.edu.iq , qais.rashck@uobasrah.edu.iq , mohw2016@stu.edu.iq
Received: 12 August 2022; Accepted: 26 September 2022; Published: 2 July 2023

Abstract

This paper presented experimental and numerical studies to investigate pressure drop in perforation horizontal wellbore with a 90° phasing and 20 spm perforation density. The experimental apparatus has been constructed to calculate the static pressure drop and calculate the exit velocity in the horizontal pipe after mixing the axial flow with the radial flow through the perforations in the wellbore. The specifications of the wellbore used were the inner diameter is 44 mm, length is 2 m, and perforation diameter is 4 mm. For this objective, a simulation model was created in the wellbore using the ANSYS Fluent simulation software by using the standard *k-ε* model and applied to the (CFD) by changing the axial flow from (40-160) lit/min and constant inflow through perforations from range (0 - 80) lit/min. According to the study's findings, the increase in the radial flow through the perforations increases the total flow rate ratio and the total pressure drop and vice versa. In addition, an increase in the axial flow mixed with radial flow increases the total pressure drop, friction factor, and a decrease in productivity index. Furthermore, the percentage error of the total pressure drop between the numerical and experimental results in test 4 is about 3.83 %. It was found that the numerical and experimental results represented a good agreement about the study of the flow-through perforations at 90° angle in terms of pressure drop and productivity index, etc.

Keywords: Horizontal wellbore, Radial flow, Pressure drop, Number of perforations, Productivity index.

https://doi.org/10.33971/bjes.23.1.15

1. Introduction

Oil and gas are being recovered from both onshore and offshore drilling activities using horizontal wells in the last decade. The productivity is limited by pressure drops within the wellbore. Deep analysis is required to study the reasons for the pressure drop from the toe-end of the horizontal well to the heel-end to maintain fluid flow within the wellbore. If the pressure drop within the wellbore is significant as compared to the reservoir drawdown, the reservoir drawdown along the well length will change. Consequently, production along the well length will also change. Normally, the pressure drop within horizontal wellbores becomes important when the production rate is high that the wellbore flow reaches turbulence. Dikken [1] proposed an analytical model for a horizontal wellbore in steady-state, single-phase, and turbulent flow. The results showed that the augmentation of production rate with increasing wellbore length quickly after the well length reaches a certain critical value.

The first study of fluid mixing between internal and main flow was raised flow provided by Su and Gudmundsson [2] studied the effect of pressure drop in a wellbore partly perforated horizontally with fluid flowing through the perforations where two fluids are mixed. The total pressure drop in the horizontal wellbore is divided into four components, friction, acceleration, perforation roughness, and mixing. The pipe was subjected to an experimental study, the test pipe consists of three equal parts, each part with a length of 600 cm, and an inner diameter of 21.94 mm. Perforation with a diameter of 3 mm, a density of 12 SPF, and a 60° phasing. The results showed that the total pressure drop is higher in relation to the higher Reynolds number due to the higher punching flow rate reducing the friction pressure loss in the test pipe. Another study in this regard was conducted by Schulkes and Utvik [3] studied the experimental and theoretical analysis of the total pressure drop in a perforated horizontal pipe. The aim of the work has been to determine the effect on the pressure drop of radial inflow by experimental means. The result showed that the mixing pressure drop is around 10 % of the drop in the friction pressure and that the drop in the mixing pressure gives a negative contribution to the drop in the pressure while giving a positive contribution to the overall drop in the large inflow. In a study conducted by Ouyang et al. [4] the significance of frictional and acceleration pressure drops in horizontal wells was investigated using a single-phase wellbore model. The results showed that the acceleration pressure differential may or, at times, may not be significant in comparison with frictional pressure. Subsequently, others [5, 6, 7] continued their research, and they proposed different coupling models of the well effect of pressure drop on the productivity ratio of a horizontal wellbore

with single-phase flow. However, in some case studies, only the friction component is observed to identify the pressure drop across the wellbore. The most probable case, acceleration was considered when studying pressure drop, and other effects such as flow, mixing, etc. were ignored.

Abdulwahid et al. [8] carried out numerical simulations have been on the flow in a partly perforated pipe with inflow in a horizontal Wellbore. Three-dimensional numerical simulations on a partially perforated pipe with 150 perforations, geometrically similar to wellbore casing (12 SPF, and 60 phasing's) were presented and analyzed. Numerical simulations by commercial code CFX were also conducted with Reynolds numbers ranging from 28,773 to 90,153. The result showed that the total pressure drop increases according to a larger acceleration pressure drop due to a higher flow rate through perforations and the total pressure drop increased with an increase in the number of perforations and vice versa. In this connection, a study by Jianguang et al. [9] conducted an experimental study to calculate the effect of different perforation parameters, such as perforation diameter, and density, and to study the effect of the injection rate on the pressure drop in the horizontal well. The pipe tested in the experiment has an external diameter of 139.7 mm, an internal diameter of 124, a perforation diameter is 10-30 mm, and perforation angle is 180°, 90°, and 45°, and a perforation density of 8-24 SPM density. It was concluded from the results that with the increase of the perforation density, perforation diameter, and perforation phase, both the frictional pressure drop and the acceleration pressure drop increase, and the mixture pressure drop decreases.

Rashad et al. [10] presented a numerical study that was carried out on perforated tubes with a phase angle of 180° and 90° respectively. The calculation was carried out with ANSYS Fluent 15.01 using the k-ε (RNG) model. It concluded from the results there is no change in acceleration and frictional wall pressure between 180° and 90° perforation phasing. The total pressure drop in 90° perforation phasing has the highest value compared with 180 phasing angles due to intensified influence of mixing pressure drop.

A semi-analytical model was developed by Luo et al. [11] mainly to calculate a horizontal well's productivity index (PI) using pressure drop in addition to the wellbore. According to this study's results, a horizontal well's PI mainly relies on the interaction between Reynolds number, horizontal-well conductivity, and penetration ratio. The ratio of a high-permeability reservoir and an optimal penetration ratio might be found in the partial-penetration zone. Liu and Shan [12] presented a numerical simulation analysis on the influence of flux ration on wellbore pressure drop in perforated completed horizontal wells. The RNG (k-ε) turbulence model in computational fluid dynamics software Fluent was used to simulate the influence of wall inflow on the mainstream in perforation completion. The results of the study show that the different injection ratios, the total pressure drop of the wellbore increases with the increase of the wall injection ratio.

Mohammed et al. [13] studied the effect of the density of the perforations (number of perforations), the phase angle of the perforations, the diameter of the perforation, and the flow rate of the crude oil from the perforations on pressure drop, and then the productivity index of the vertical wellbore with two perforations, by using ANSYS Fluent 15.0 to simulate a model of 3-D turbulent flow with standard (k-ε) in a perforated vertical wellbore. The results of this study show that increased perforation density of the perforated vertical wellbore caused an increase in pressure drop and decreased productivity index due to increasing friction losses.

The purpose of this research is to determine the major differences between experimental and numerical results that emphasize the effect of pressure drop along the perforated pipe. It also intends to use mathematical formulae to calculate the influence of pressure drop (mixing, acceleration, and friction), friction factor, and productivity index. Also, attempted to evaluate the effect of the through-perforation flow rate relative to the main flow on the horizontal well productivity index. The following is how this paper is organized. The authors begin with some theoretical background information for an experimental device. The details of the numerical model and geometry were then presented, as well as a discussion of the essential parameters influencing pressure loss in horizontal wellbore.

2. Experimental work

Experiments were mainly conducted to determine the static pressure drop, due to the change in flow rate through the well and the change in flow rate through the perforation. In addition, this paper also studies the productivity index and how it affects oil production in horizontal wells. Moreover, a special test section is made into a ring horizontal flow. The flow loop diagram is shown in Fig. 1 and the test pipe is obviously shown in Fig. 2.

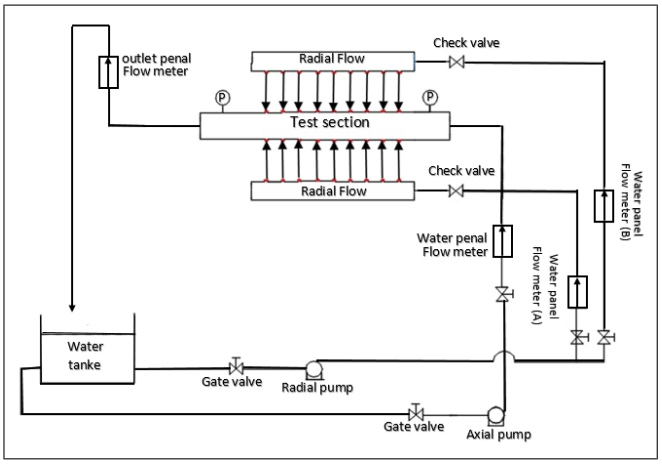

Fig. 1 the experiment apparatus's schematic diagram.

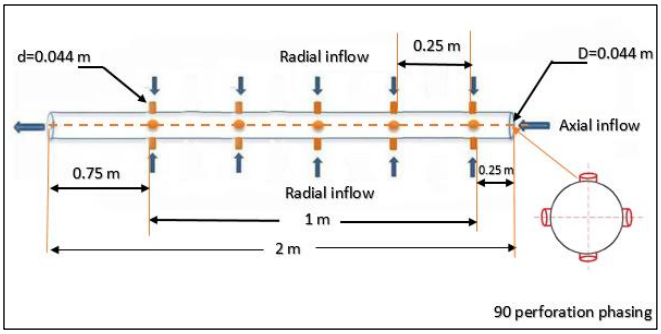

Fig. 2 the test pipe's schematic diagram.

This study's experimental apparatus embodied two loops of water circulation that is, the first loop works to supply water to the main pipe, while the other loop is used for the test pipe.

The test pipe is ultimately filled with water through the perforations.

The pipe is made from PVC has 2 m length, 50 mm outer diameter along 44 mm inner diameter. The test pipe is perforated with 20 perforations and a perforations angle of 90°. The pipe is divided into three parts. The length of the perforated part is 1 m, and the length of the blank section is 0.25 m before the perforated section, and the length of the blank section is 0.75 m after the perforated section. The perforation diameter is 4 mm and the length of the perforation from the surface of the test pipe is 0.003 mm. Besides, the parameters of the main instruments are listed in Table 1.

Table 1. the main instrument's parameters

Device	Tool specifications	Measurement range
Water panel flowmeter in the main pipe	PVC (0.0127 m)	(40 - 160) Lit/min
Water panel flowmeter in inflow through perforations	PVC (0.0127 m)	(0.6 - 6) Lit/min
Pressure sensor gauge	Stainless stales G1/4 NPT (male) (4-20 mA)	(0 - 1.2) MPa
Axial pump	CPm 158 (2 HP)	(50 – 750) Lit/min
Radial pump	Dcd 20 (2 HP)	(30 – 500) Lit/min
Gate valve, check valve	PVC (0.0127 m)	-
Water storage tank	PVC	(1/2) ton

The experimental apparatus is consisting of two pressure sensors, one before perforation and the other after perforation at a distance of 0.15 cm from each side of the pipe. Besides, the static pressure drop in the test pipe was calculated by means of the pressure sensors. The pressure sensor has been connected to the Arduino and the Arduino has been linked to a screen in order to display the static pressure for each point or in the image of the difference between two points.

3. Numerical simulations

The rapid advancement of computer technologies and software enables the solution of theoretical simulations for complex applications. This paper investigates a numerical analysis of a single-phase flow through a horizontal wellbore. The mathematical simulation with a 3D model with turbulent flow in the horizontal wellbore is performed using CFD ANSYS Fluent. The horizontal wellbore simulation is carried out using the conservation law (mass, and momentum) in conjunction with the perturbation (k-ε) model. The finite volume method (FVM) solution of the continuity, momentum, and turbulence model equations is used to explain the calculation process of the control differential equation.

4. Description of the models

The numerical analysis is performed using ANSYS Fluent and the standard k-ε model. The three-dimensional geometry of the horizontal well pipes is made of PVC with perforations surface roughness of 0.03 mm. The inner diameter of the pipe is 0.044 m, and the length is 2 m. The first pipe is 20 perforations divided into two lines with 90° perforation phasing for each line has 5 perforations. Figure 3 shows the physical model of the perforation pipe.

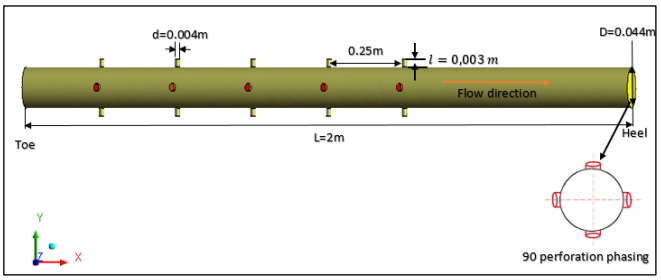

Fig. 3 the physical model for 90° perforation phasing.

5. Simulation parameters

The fluid considered for the simulations is water with constant density of 998.2 kg/m^3 and dynamic viscosity of 0.001 kg/ms. In each of the tests, flow rate through the perforations was increased from zero to maximum value. The roughness of the test pipe wall was 0.03 mm, the type of the test pipe was PVC. Test details are summarized in Table 2. Uniform water mass flow is introduced at the inlet of a partially perforated pipe. Two boundary conditions are considered. At the inlet mass flow is taken into consideration both axially and radially whereas at the exit outlet pressure is zero considered as the boundary condition. It is assumed that no-slip boundary conditions occur along the walls. The work was done under conditions of temperature from 23-25 °C.

The assumptions of the present are the phase is single, turbulent flow, steady state flow, Newtonian fluid, incompressible flow, and there is no transfer of heat between the system and its surrounding.

Tests are performed at different flow rates of the axial flow, and radial flow through the perforations with an interval value of 6.6 Lit/min for each test as shown in Table 2.

Table 2. the details of the flow.

Flow Test	Axial flow (Lit/min)	Radial flow (Lit/min)
Test 1	40	0 - 80
Test 2	80	0 - 80
Test 3	120	0 - 80
Test 4	160	0 - 80

5.1. Governing equations

Fluid flow in perforated horizontal wellbore undergoes a considerable measure of physical changes such as pressure. The change of the pressure is due to friction losses in horizontal pipe and perforations, mixing, acceleration and gravity, velocity change caused by varying flow regimes, and density. In order to properly describe these physical changes, we need to solve the two governing equations of fluid flow (mass and momentum equations). The mathematical statements representation of the conservation of physical laws is given below [14, 15 and 16].

5.1.1. Conservation of mass

Based on the mass balance for the fluid element, we can derive the conservation of mass equation which is given as [16].

$$\rho \frac{\partial}{\partial x_i}(u_i) = 0 \tag{1}$$

For turbulent flow, breaking the instantaneous velocity into mean and fluctuating components is defined as:

$$u_i = \bar{u}_i + u_i' \tag{2}$$

Where,
$\bar{u}_i$: the mean velocity vector.
u_i' : the fluctuating velocity vector.

5.1.2. Conservation of momentum

In general, the momentum conservation equation is represented in Cartesian coordinates as follows:

$$\frac{\partial}{\partial t}(\rho u_i) + u_j \frac{\partial(\rho u_i)}{\partial x_j} = -\frac{\partial P}{\partial x_i} + \frac{\partial}{\partial x_j}(\tau_{ji}) + F_i \tag{3}$$

The viscous stress tensor can be rewritten in terms of the strain rate tensor by:

$$\tau_{ji} = \mu \left(\frac{\partial u_j}{\partial x_i} + \frac{\partial u_i}{\partial x_j} \right) = 2\,\mu\, S_{ji} \tag{4}$$

τ_{ji} : the viscous stress tensor.
S_{ji} : the strain rate tensor (rates of deformation of a fluid).

In turbulent flow, the instantaneous quantities can be broken up into mean and fluctuating components.

$$\begin{aligned} u_i &= \bar{u}_l + u_i' \, u_j = \bar{u}_j + u_j' \, P = \bar{P} + P' \\ S_{ji} &= \bar{S}_{ji} + S'_{ji} \end{aligned} \tag{5}$$

Substituting Eq. (5) into Eq. (3) and taking the time-averaged, yields the momentum equation for incompressible flow. Typically called Reynolds-averaged Navier-Stokes.

$$\rho \bar{u}_j \frac{\partial}{\partial x_j}(\bar{u}_i) = -\frac{\partial \bar{P}}{\partial x_i} + \frac{\partial}{\partial x_j}\left(2\,\mu\, \bar{S}_{ji} - \rho\, u_i' u_j'\right) + F_i \tag{6}$$

Typically referred to as Reynolds-averaged Navier-Stokes. To calculate the Reynolds stresses, employ the well-known Boussinesq relationship:

$$\rho \overline{u_i' u_j'} = \frac{2}{3} k\, \delta_{ij} - \mu_t \left(\frac{\partial \bar{u}_j}{\partial x_i} + \frac{\partial \bar{u}_i}{\partial x_j} \right) \tag{7}$$

Where:
δ_{ij} : represents the kronecker delta,
$\delta_{ij} = 1$ if $i = j$ and $\delta_{ij} = 0$ if $i \neq j$

5.2. Models of turbulence (standard k-ε model)

The standard *k-ε* model belongs to the general group of two-equation models, which tackle two separate transport equations and they are the most widely used in industrial applications because of it provides economy, robustness and reasonable accuracy. The standard *k-ε* model uses the following transport equations for *k*.

$$\rho u_j \frac{\partial k}{\partial x_j} = \frac{\partial k}{\partial x_j}\left(\left(\mu + \frac{\mu_t}{\sigma_k} \right) \frac{\partial k}{\partial x_j} \right) + 2\,\mu_t\, S_{ij}\, S_{ij} - \rho\varepsilon \tag{8}$$

and for ε:

$$\rho u_j \frac{\partial \varepsilon}{\partial x_j} = \frac{\partial \varepsilon}{\partial x_j}\left(\left(\mu + \frac{\mu_t}{\sigma_\varepsilon} \right) \frac{\partial \varepsilon}{\partial x_j} \right) + C_{1\varepsilon} \frac{\varepsilon}{k}\, \mu_t\, S_{ij}\, S_{ij} - C_{2\varepsilon}\, \rho \frac{\varepsilon^2}{k} \tag{9}$$

The strain rate's tensor can be expressed as per velocity.

$$S_{ji} = \frac{1}{2}\left(\frac{\partial u_j}{\partial x_i} + \frac{\partial u_i}{\partial x_j} \right) \tag{10}$$

Besides, the terms of the boundary of the equation *k-ε* are listed in Table 3.

Table 3. Boundary conditions for the (*k-ε*) model.

Inlet	$K = \frac{3}{2} I^2 U^2 \quad , \quad \varepsilon = \frac{K^{0.5}}{0.3\, D_h}$ I : is the specified turbulence intensity. D_h :is the hydraulic diameter of the inlet.
Outlet symmetry axis	$\partial k/\partial n = 0$ and $\partial \varepsilon/\partial n = 0$

The input is based on the mean value of the intensity is 5% and the viscosity ratio μ/μ_t equal to 10.

The constants were determined by fitting data intensively to the standard model *k*-ε for a wide range of turbulent flows. These equations include some constants [16]:

Table 4. standard constants for the (k-ε) model.

Constants	C_μ	σ_k	σ_ε	$C_{1\varepsilon}$	$C_{2\varepsilon}$
Values	0.09	1.00	1.3	1.44	1.92

6. Theoretical model

6.1. Total pressure drop

The total pressure drop in a perforated horizontal wellbore can be divided into three sources, as given by the following relationship.

$$\Delta P_T = \Delta P_f + \Delta P_{mix} + \Delta P_{acc.} \tag{11}$$

This can be rearranged using the above equations to obtain the total pressure drop.

$$P_{in} - P_{out} = \rho(u_{out}^2 - u_{in}^2) + \Delta P_{wall} + \Delta mix \tag{12}$$

According to Eq. (12), the total pressure drop consists of three distinct components:

1. Pressure drop as a result of kinematic energy change (acceleration effects). This demonstrates the first term on Equation's right side (12).

$$\Delta P_{acc.} = \rho\ (u_{out}^2 - u_{in}^2) \tag{13}$$

Where u_{in} , u_{out} the average velocity of the fluid, at both the inlet as well as the outlet of the pipe, respectively.

2. The frictional pressure drop due to wall friction and perforation roughness, ΔP wall, is based on the average velocity u_{out} downstream of the perforation and can be calculated from the Darcy-Weisbach equation [13, 17, and 18].

$$\Delta P_f = f_t \frac{\Delta L}{D} \frac{\rho\, u_{out}^2}{2} \tag{14}$$

The total friction factor quantifies the force produced by the fluid on the wall in a turbulent flow. The equation can be used to compute the friction factor.

$$f_t = f_o + f_p \tag{15}$$

f_t : represents the total friction factor for the pipe (dimensionless).
D: represents the main pipe's diameter (m).
L: length of pipe.

When the relative roughness of the pipe is known, the Haaland equation provides an accurate and convenient relationship for the friction factor in turbulent pipe flow [19].

$$\frac{1}{\sqrt{f_0}} = -\,1.8 \log\left(\frac{6.91}{Re} + \left(\frac{\epsilon}{3.7D}\right)^{1.11}\right) \tag{16}$$

The Reynold number is used to describe the ratio of inertia to viscous force. The friction factor of unperforated wellbore is calculated using the equation below.

$$Re = \frac{\rho\, u_{out}\, D}{\mu} \tag{17}$$

In fact, Asheim et al. [20] provided a mathematical model which is mainly intended to determine the effective friction factor owing to inflow through perforations, using the equation below.

$$f_p = 4D\left(\frac{q}{Q_{out}}\right) + 2\frac{D}{n}\left(\frac{q}{Q_{out}}\right)^2 \tag{18}$$

The radial flow through perforation is calculated using the following equation:

$$q = n\frac{\pi}{4} d^2\, U_2 \tag{19}$$

q/Q_{out} : the total flow rate ratio can be defining as the ratio of the radial flow (inflow through perforation) to the total flow rate of the outlet main pipe.

3. The pressure drop caused by mixing effects ΔP_{mix}, is an irreversible pressure drop that cannot be described further. The complicated interaction between perforation flow and wellbore flow, which generates disturbances in the boundary layer and hence influences the pressure drop, causes this pressure effect. The irreversible pressure drop due to mixing needs to be determined by experiments. Moreover, when the ratio's flow rate becomes greater than 0.0025, we can calculate the mixing pressure drop, using equations developed by Su and Gudmundsson [18, 21]

$$\Delta P_{mix} = 760\left(\frac{q_i}{Q_{out}}\right) \tag{20}$$

6.2. Productivity index

The productivity index (PI) is calculated using a mathematical equation derived from dividing the main pipe's outflow by the total drop in pressure denoted by the symbol PI (m^3/s)/kPa, as follows.

$$Pi = \frac{Q_{out}}{\Delta P_T} \tag{21}$$

7. Grid independence test

In order to ensure the grid-independent solution, the first step of the numerical simulation is identifying the maximum mesh size, which is used to solve in ANSYS Fluent 15.0 commercial software. Varying the maximum size of the mesh is applied to show the best mesh properties which can be used to simulate the cases in a present study. A tetrahedron is used to generate the mesh with different maximum mesh sizes. Three boundary layers are used on the wall of the pipe. Fig. 4 shows the structured computational grids.

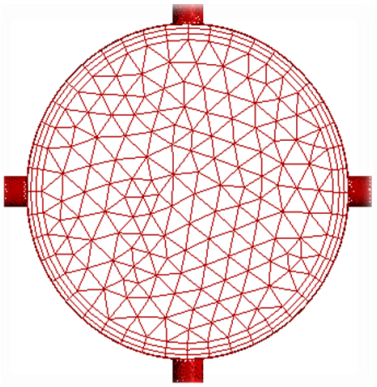

Fig. 4 Cross geometry of the test pipe.

The grid independence of all the mesh sizes is based on the average static pressure at two locations, the first location at a centerline along (x-axis) and the second location at the fluid domain as shown in Fig. 5.

The minimum percentage error of the predicted average static pressure lies between the previous and the next of the maximum mesh size of 0.00315 mm with 275394 nodes and 1063960 elements. The percentage error between grid 17 and grid 18 for the two locations is 0.04 % for the centerline along (x-axis), 0.017 % for the fluid domain. The maximum mesh size of 0.00315 mm is used in the simulation in order to obtained good accuracy results. For checking quality, the determinant of an element obtained is equal to 0.79 at least.

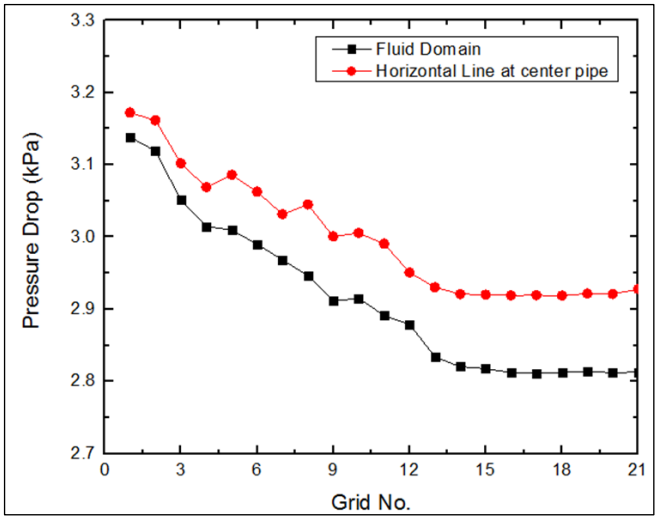

Fig. 5 Comparison of the average static pressure for varying mesh size.

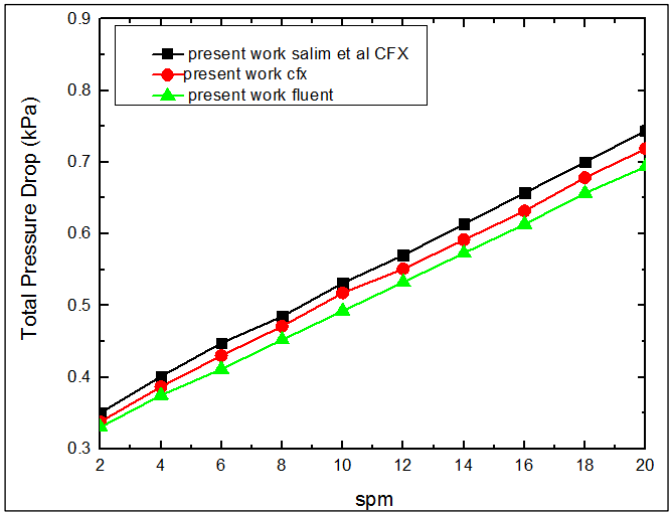

Fig. 7 Validation of present work with Salim et al. [18].

8. Model validation

In order to verify the accuracy of the numerical results of the current work. A comparison with the results of Salim et al. [18] is performed. They used CFD to simulate a perforated well. A three-dimensional well with multi-perforation as shown in Fig. 6. The length of the well is 1 m and the diameter is 0.2 m. The perforation length is 0.15 m, the diameter is 0.012 m and the 180° phase angle.

The boundary conditions for this validation are as follows, the inlet velocity is 2.5 m/s, while the velocity from each perforation is 1 m/s and the static pressure at the well outlet is equal to zero. The wall is smooth, has a no-slip boundary, and neglects the effect of gravity.

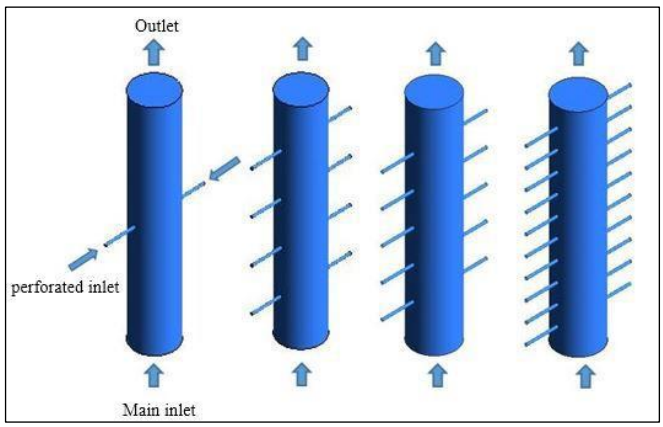

Fig. 6 Geometry of perforated vertical wellbore with multi-perforation with 180º.

The ANSYS CFX 15.0 and Fluent with turbulence models stander (k-ε) model are used to simulate, the steady-state, incompressible, and 3D fluid flow. The results of this validation for the total pressure drop to all were cases very acceptable, as shown in Fig. 7. The maximum errors between Salim et al. [18] and the current work using ANSYS CFX 15.0 is less than 3.5 %, while by using Fluent the maximum error increase of about 5.8 %.

9. Results and discussion

In this paper, an experimental study is conducted and the experimental results are compared with the numerical results on the perforated pipe. To determine the overall pressure drop and the static pressure as a result of the change in axial and radial flow. In addition, a study at evident friction factors, productivity indices, and velocity profiles is in order. The study is carried out at various flow rates, as shown in Table 2.

9.1. Total pressure drop

Figure 8 illustrates the comparison between the total pressure drop and total flow rate ratio. The total pressure drop is calculated by taking the static pressure drop reading from the pressure sensor and comparing it with the numerical values calculated from the ANSYS Fluent CFD program and applying the theoretical Eq. (11) to calculate the total pressure drop for a variety of axial and radial flow rates. According to the figure, the total pressure drop increases as the total flow rate ratio increases. As a result of the higher flow rate through the perforations, there is a higher acceleration pressure drop. At each increase in flow through the perforations, the outlet velocity in the main pipe of the experimental apparatus is calculated. In addition, it was found that increased wall friction was caused by increased average flow velocity due to inflow through the perforations and the increase in the mixing effect resulting from mixing the axial flow with the radial. The percentage error between experimental and numerical in the several flow tests is 4.52 %, 7.22 %, 8.55 %, and 3.83 %, respectively.

Figures 9 and 10 represent the relationship between pressure drop and the total flow rate ratio. It is found that the total pressure drop increases with increasing the total flow rate ratio. The proportion of the flow rate increases as the rate of the flow-through perforations increases, and the overall pressure drop increases. The main reason is that the higher flow rate through the perforations results in a greater decrease in the acceleration pressure caused by the flow through the perforations, thus increasing the mixing effect. It is observed that the acceleration values are lower in the wellbore pressure drop than the frictional pressure drops in resulting (wall friction and perforation roughness). For the experimental results, the wall friction pressure drop is about 62.4 % of the overall pressure drop, and the acceleration pressure drop is 35%, and the mixing pressure drop 2.6 %. While the numerical

results, the friction pressure drop is about 69.5 %, and 27.7 % acceleration pressure drop and mixing pressure drop 2.8 %.

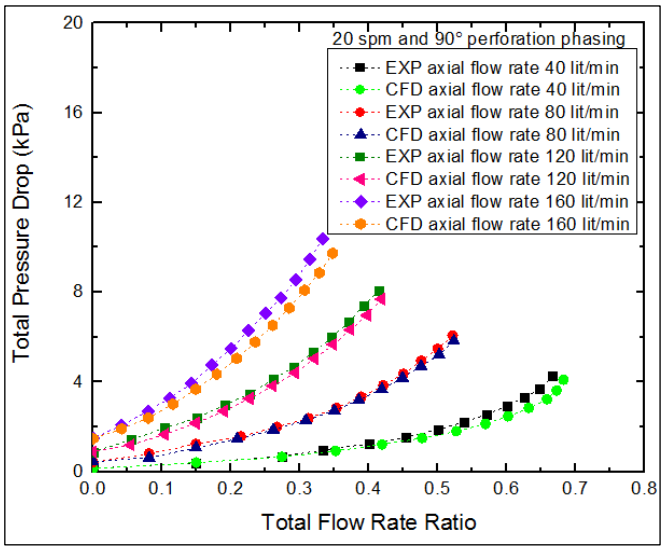

Fig. 8 Comparison between the experimental and numerical results of the total pressure drop.

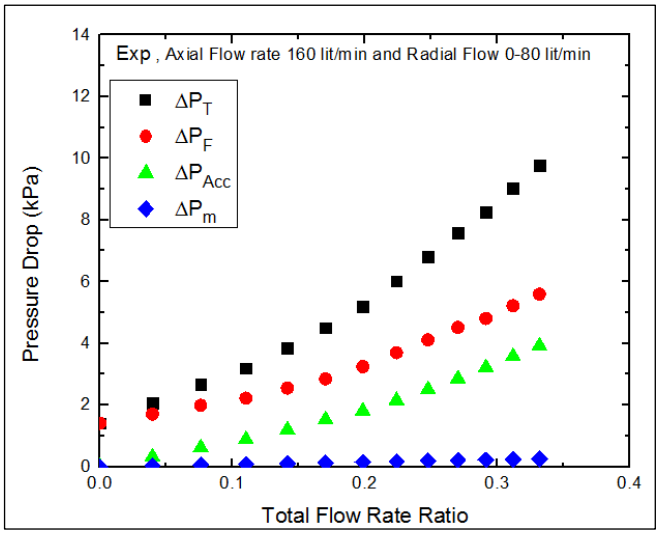

Fig. 9 Experimental results of the pressure drop.

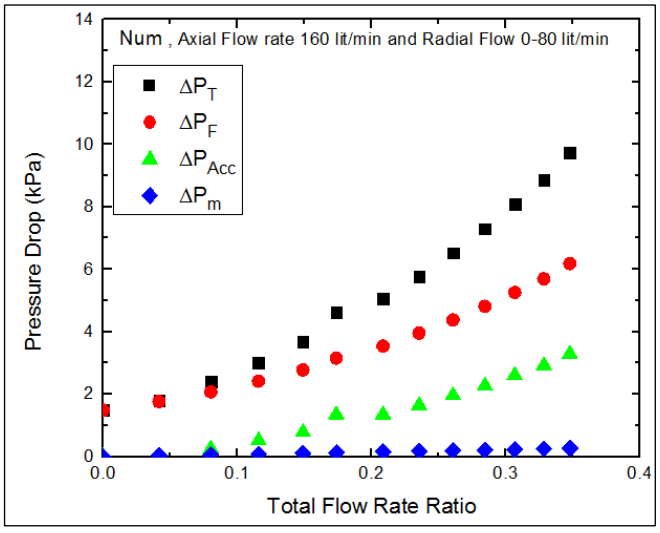

Fig. 10 Numerical results of the total pressure drop.

9.2. Static pressure drop

Figure 11 represents the relationship between static pressure drop and total flow rate ratio when the perforation density is equal to 20 spm and 90° perforation phasing. The static pressure drop is represented from the experimental by taking the reading from the pressure sensor and comparing the experimental reading with the numerical data which computed from the CFD ANSYS Fluent programs for several flow rates. It is shown from the figure the static pressure drop increase as the flow rate ratio increases (an increase of radial flow through perforation for the axial flow through pipe remains constant). The static pressure drop increases with increasing in Reynolds number, this is due to high velocity this rise in friction pressure is a result of the effect of the shear stress on the wall and consequently the increase in the flow rate as a result of flowing through the perforation. The percentage error between experimental and numerical in the axial flow test 40, 80, 120, 160 Lit/min and the change radial flow from 0 - 80 Lit/min is 5.52 %, 4.22 %, 6.55 %, and 5.83 %, respectively.

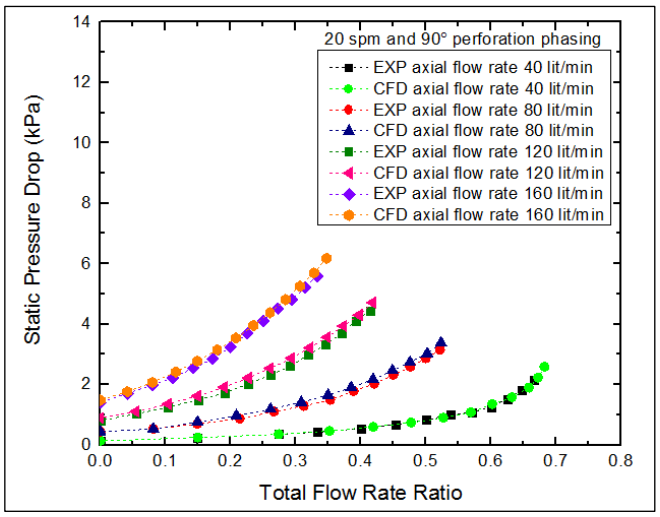

Fig. 11 Comparison between the experimental and numerical results of a static pressure drop.

Figure 12 represents the static pressure contour distribution along 2 m horizontal wellbore as the axial flow becomes 160 Lit/min and the radial flow is 80 Lit/min. This figure shows that the pressure decreases gradually from the toe of the well to the heel of the well. Because the pressure gradient begins decreasing in the area where the flow through the perforations meets the radial flow and continues to decrease to the end of the pipe.

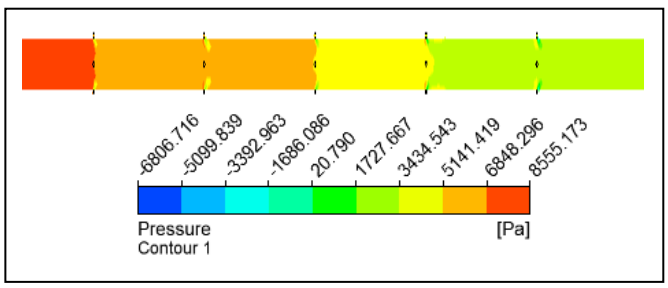

Fig. 13 the contours of pressure distribution along the pipe.

Figure 14 demonstrates the pressure drop on the polyline that is created from the intersection of the wall of the pipe and the vertical plane at the center of the pipe. The axial flow is 40, and 160 Lit/min, and the constant radial flow is 80 Lit/min. It is noted that there is a decrease in pressure near the perforation from upstream to downstream and is gradually recovering after perforation. The pressure drop is almost completely restored to its original state before the fluid exits the pipe. In addition, the pressure rises in the upper part of the pipe surface and decreases in the lower part of the surface. The pressure oscillation occurs through the perforation area as a result of the effect of the perforations. The results also showed that the pressure at the end of the heel will be lower compared to the total pressure in the toe.

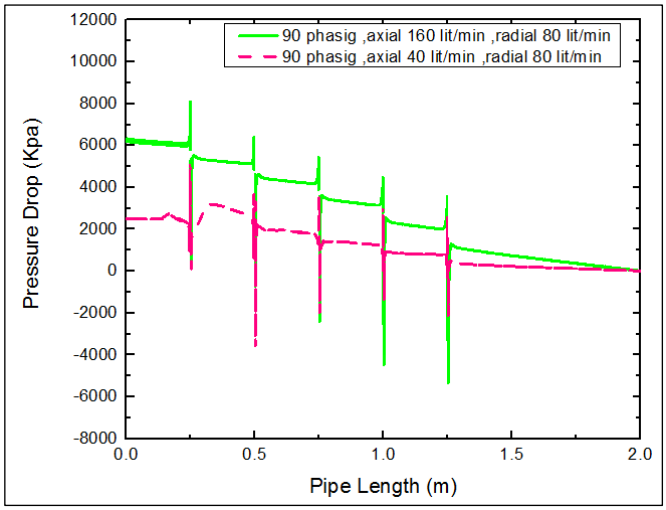

Fig. 14 Distribution of the static pressure on up and down part of the wellbore in the 90° perforation phasing.

9.3. Apparent friction factor

Using the exit velocity and friction pressure drop measured in the experimental results, the apparent friction factor is calculated from the friction pressure drop, flow rate, and pipe length according to Eq. (15). The variation of the apparent friction factor, when comparing the experimental and numerical with a different radial flow rate is shown in Fig. 15. This occurs because the apparent friction factor increases with increasing Reynolds number, which results in a large velocity difference as a result of a high flow Reynolds number combined with wall pipe roughness. This high velocity causes high shear stress on the wall. It is noted from the figure that the friction factor has higher numerical results than experimental results, the experimental results are unstable for the type of turbulent flow, and therefore the reading of the friction pressure gauge fluctuated the experimental reading has every increased in the axial and radial flow rate. The Reynolds numbers are based on four test lines for axial flow: 40, 80, 120, and 160 Lit/min, and a radial flow change from 20 to 80 Lit/min. The percentage error between experimental and numerical in the several flow tests is 6.81 %, 7.62 %, 7.95 %, and 4.54 %, respectively.

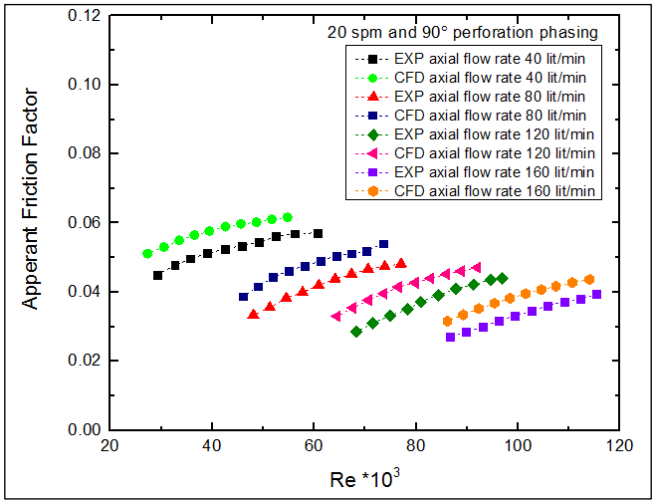

Fig. 15 Comparison between the experimental and numerical apparent friction factor with Reynold number.

9.4. Productivity index

Figure 16 shows the comparison results between the experimental and the numerical productivity index with the total flow rate ratio at 90° perforation phasing. According to the figure, the resulting productivity index is based on theoretical calculations according to Eq. (21) and through the flow rate out of the pipe in the experimental device and theoretically and experimentally calculated the total pressure drop. It is noticed from the figure that the results obtained by the ANSYS program are higher than the values obtained experimentally because the experimental results are unstable. The productivity index decreases with the increase in the total flow rate ratio. As a result of the flow through the perforations, there is a fundamental change in velocity coming out of the main pipe. Due to the pressure energy consumed, the fluid flow increases, and the total pressure drop increases. The productivity index decreases as a result.

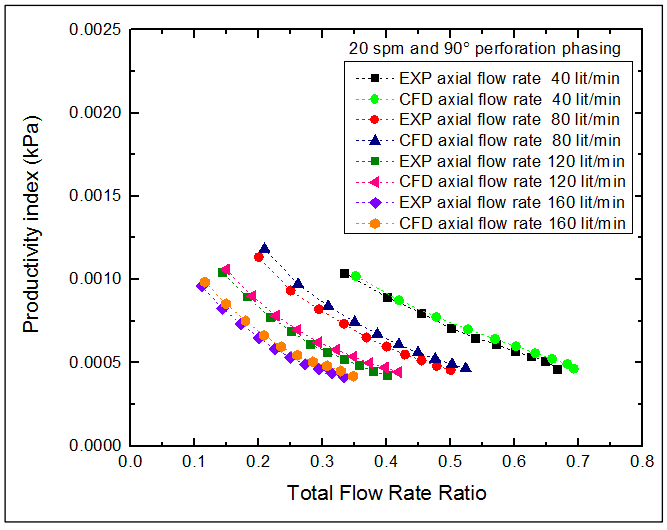

Fig. 16 Comparison between the experimental and numerical result of productivity index for different total flow rate ratio.

9.5. Average velocity in the center-line of perforation pipe

Figure 17 represents the relationship between the maximum velocity of the center-line of the pipe length in the test line for constant radial flow 80 Lit/min and defines axial flow in Table 2. It is observed that the flow in the perforation disrupts the axial flow in the pipe, and this lead to increase in the velocity in the wellbore pierced from the toe tip to the heel tip due to the radial flow entering through the perforation as shown in Fig. 18. This figure explains the contour velocity distribution along the length pipe when the axial flow is 160 Lit/min and the radial flow is 80 Lit/min.

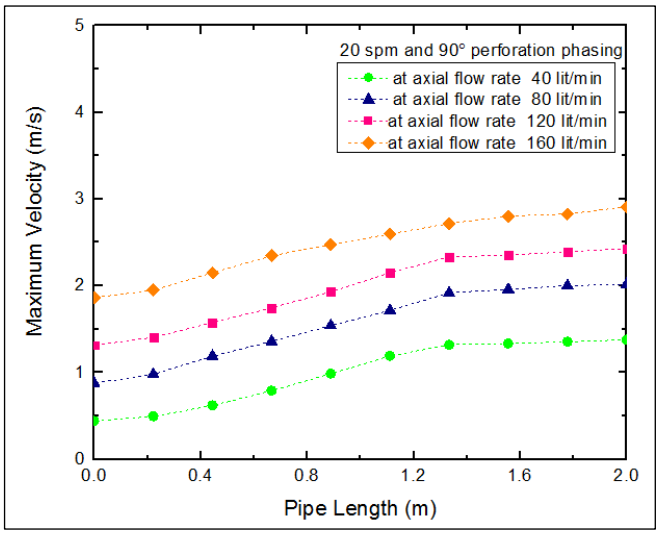

Fig. 17 the maximum velocity along the pipe length for different axial flow rate.

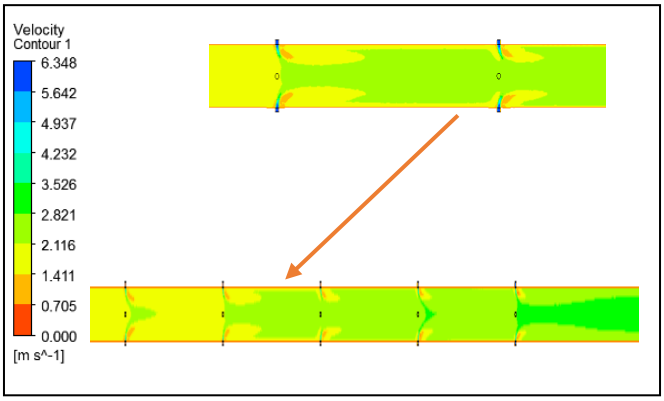

Fig. 18 the contours of velocity distribution along the pipe length.

Figure 19 explains the velocity vector distribution of the planes along the pipe at the end of the perforation section located at 1.3 m for the perforation phasing 90°. When the axial flow change of 40, 80,100, 120, and 160 Lit/min respectively, and a radial flow of 20 Lit/min. The figure also shows that the velocity is lowest at the wall and improves gradually to the maximum at the center of the pipe. As water pressure pushing the flow increases, flow within the pipe becomes more turbulent.

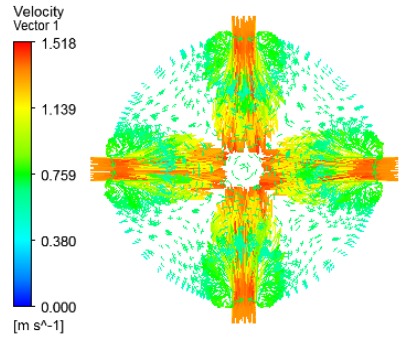

(a) At axial flow rate 40 Lit/min.

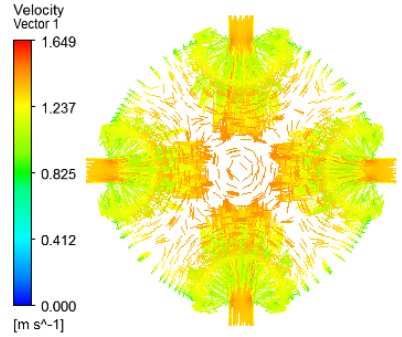

(b) At axial flow rate 80 Lit/min.

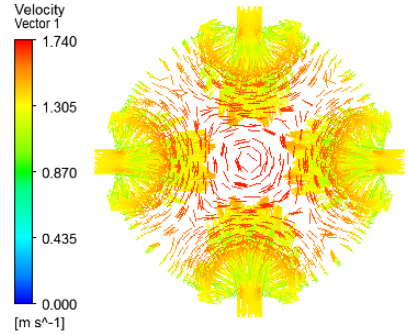

(c) At axial flow rate 120 Lit/min.

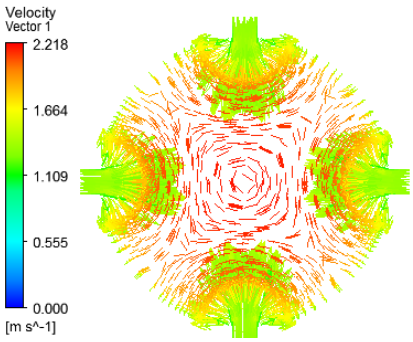

(d) At axial flow rate 160 Lit/min.

Fig. 19 Vectors of velocity for the end perforation section of the 90° perforation phasing at the *y*-*z* plane.

10. Conclusions

An experimental and numerical study is conducted on perforation pipe with inflow during perforations in the horizontal wellbore. The experimental results were calculated from the device and obtained from the equations and compared with the numerical results for different flow rates in axial flow and inflow through the perforation. The numerical simulation of a perforation horizontal wellbore has been examined using ANSYS fluent using the standard *k*-ε model. It is noted that the

numerical results are slightly higher than the experimental results. The study shows the following conclusions:

1. The total pressure drop between the experimental values is higher than the numerical.
2. There is good agreement in the static pressure drop at the increase in the total flow rate ratio between the values measured from the experimental and numerical using ANSYS Fluent.
3. The total pressure drop in the experimental increases as the axial velocity increases. While increasing the radial velocity in the experiment leads to a slight increase in the total pressure drop.
4. For a wellbore that is fully perforated, the pressure drop caused by friction is much higher than the pressure drop caused by acceleration. There is a minimal effect of the mixing pressure drop on the total pressure drop.
5. There is a small difference between the experimental and numerical productivity indexes.
6. The maximum velocity increases with an increase in axial flow, but inflow through the perforations remains constant, and the maximum velocity occurs at the end of the pipe due to the effects of the perforations.

Nomenclature		
Symbol	**Description**	**SI Units**
A	Area	m^2
D	Wellbore diameter	m
d	Perforation diameter	m
F	Friction Factor	
K	The turbulent fluctuations of the kinetic energy	
L	Wellbore length	m
N	Perforation density	spm
Q	Axial flow	m^3/s
Q_{out}	Total flow rate of the outlet main pipe	m^3/s
q	Radial flow through the perforation	m^3/s
u_{out}	The average velocity at the outlet of the wellbore	m/s
u_i , v_i	Velocity vector component	m/s
ΔP	Pressure drop	kPa
	Greek Symbols	
Symbol	**Description**	**SI Unit**
ϵ	Roughness	m
μ	Fluid viscosity	kg/m.s
ρ	Density	kg/m^3
ε	Turbulent dissipation rate	m^2/s^3
σ	Stefan-Boltzmann constant	$W/m^2 K^4$
μ_t	Eddy viscosity is also known as turbulent viscosity.	kg/m.s

References

[1] B. J. Dikken, "Pressure Drop in Horizontal Wells and Its Effect on Production Performance", Journal of Petroleum Technology, Vol. 42, Issue 11, pp. 1426-1433, 1990. https://doi.org/10.2118/19824-PA

[2] Z. Su, and J. S. Gudmundsson, "Pressure Drop in Perforated Pipes: Experiments and Analysis", SPE Asia Pacific Oil and Gas Conference, Melbourne, Australia, November 7-10, 1994. https://doi.org/10.2118/28800-MS

[3] R. M. S. M. Schulkes, and H. O. Utvik, "Pressure Drop in a Perforated Pipe with Radial Inflow: Single-Phase Flow", SPE Journal, Vol. 3, Issue 1, pp. 77-85, 1998. https://doi.org/10.2118/38448-PA

[4] L. B. Ouyang, S. Arbabi, K. Aziz, "A Single-Phase Wellbore-Flow Model for Horizontal, Vertical, and Slanted Wells", SPE Journal, Vol. 3, Issue 2, pp. 124-133, 1998. https://doi.org/10.2118/36608-PA

[5] E. Ozkan, C. Sarica and M. Haci, "Influence of Pressure Drop Along the Wellbore on Horizontal-Well Productivity", SPE Journal, Vol. 4, Issue 3, pp. 288-301, 1999. https://doi.org/10.2118/57687-PA

[6] W. Campos, R. C. Aguiar and D. Lopes, "Frictional and Accelerating Pressure Drops Effects on Horizontal Oil Well Productivity Index", 18th International Congress of Mechanical Engineering, November 6-11, 2005.

[7] F. Zeboudj and L. Bahi, "Horizontal Well Performance Flow Simulation CFD-Application", SPE Production and Operations Conference and Exhibition, Tunis, Tunisia, June 2010. https://doi.org/10.2118/133269-MS

[8] M. A. Abdulwahid, and S. F. Dakhil, "Numerical analysis of fluid flow properties in a partially perforated horizontal wellbore", American Journal of Energy Engineering, Vol. 2, Issue 6, pp. 133-140, 2014. https://doi.org/10.11648/j.ajee.20140206.12

[9] W. Jianguang, L. Xuesong, L. Xuemei and M. Yuanyuan, "The Experimental and Model Study on Variable Mass Flow for Horizontal Wells with Perforated Completion", Journal of Energy Resources Technology, Vol. 139, Issue 6, 2017. https://doi.org/10.1115/1.4037026

[10] Z. M. Rashad, M. A. Abdulwahid and Q. A. Rishak, "Comparison of Pressure Drop in Horizontal Wellbore for 90° and 180° Perforation Phasing", Seventh International Conference on Advances in Civil, Structural and Mechanical-CSM 2018, pp. 62-67, 27-28 October, 2018. https://doi.org/10.15224/978-1-63248-163-4-36

[11] W. Luo, C. Tang and Y. Feng, "A Semi Analytical Model for Horizontal-Well Productivity with Pressure Drop Along the Wellbore", SPE Journal, Vol. 23, Issue 5, pp. 1603-1614, 2018. https://doi.org/10.2118/189973-PA

[12] Ss. Liu, "Numerical Simulation Analysis on the Influence of Wall Inflow on Main Stream in Perforation Completion", International Petroleum and Petrochemical Technology Conference, Springer, Singapore, pp. 232-240, 2020. https://doi.org/10.1007/978-981-16-1123-0_24

[13] H. S. Mohammed, E. A. Khazal and H. S. Sultan, "Studying the Effect of Perforation Parameters on Vertical Well Performance", Basrah Journal for Engineering Sciences, Vol. 20, No. 2, pp.48-59, 2020. https://doi.org/10.33971/bjes.20.2.6

[14] H. S. Mohammed, H. S. Sultan and E. A. Khazal, "Simulation of a Perforated Vertical Wellbore with Near Wall Porous Media Effect", Journal of Petroleum Research and Studies, Vol. 12, No. 1, Issue 34, Part 1, pp. 85-104, 2022. https://doi.org/10.52716/jprs.v12i1.592

[15] A. J. Al-Husseini, F. A. Abood and A. K. Alshara, "Hydrodynamics Behavior of Single and Multi-Fracture with Different Orientations in Petroleum Reservoir", Basrah Journal for Engineering Sciences, Vol. 19, No. 1, pp. 12-16, 2019. https://doi.org/10.33971/bjes.19.1.2

[16] H. K. Versteeg, W. Malalasekera, "An Introduction to Computational Fluid Dynamics", Second edition, Prentice Hall, 2007.

[17] L. Hua, L. Yan, P. Xiaodong, L. Xindong, W. Laichao, "Pressure Drop Calculation Models of Wellbore Fluid in Perforated Completion Horizontal Wells", International Journal of Heat and Technology, Vol. 34, No. 1, pp. 65-72, 2016. https://doi.org/10.18280/ijht.340110

[18] M. K. Salim, H. S. Sultan and A. K. M. AL-Share, "Effect of Shape and Parameters of Perforation in a Vertical Wellbore with Two Perforations (without Porous Media) on Pressure Drop", Fluid Mechanics: Open Access, Vol. 4, Issue 3, 2017. https://doi.org/10.4172/2476-2296.1000162

[19] S. E. Haaland, "Simple and Explicit Formulas for the Friction Factor in Turbulent Pipe Flow", Journal of Fluids Engineering, Vol. 105, Issue 1, pp. 89-90, 1983. https://doi.org/10.1115/1.3240948

[20] H. Asheim, J. Kolnes, and P. Oudeman, "A Flow Resistance Correlation for Completed Wellbore", Journal of Petroleum Science and Engineering, Vol. 8, Issue 2, pp. 97-104, 1992. https://doi.org/10.1016/0920-4105(92)90048-6

[21] Z. Su, and J. S. Gudmundsson, "Perforation Inflow Reduces Frictional Pressure Loss in Horizontal Wellbores", Journal of Petroleum Science and Engineering, Vol. 19, Issue 3-4, pp. 223-232, 1998. https://doi.org/10.1016/S0920-4105(97)00047-8